Nearest-neighbor sp(3)d(5)s* tight-binding parameters based on the hybrid quasi-particle self-consistent GW method verified by modeling of type-II superlattices

Sawamura, Akitaka
Otsuka, Jun
Kato, Takashi
Kotani, Takao
Souma, Satofumi

(Citation)
Optical Materials Express,8(6):1569-1584

(Issue Date)
2018-06-01

(Resource Type)
journal article

(Version)
Version of Record

(URL)
https://hdl.handle.net/20.500.14094/90004956

Research Article | Vol. 8, No. 6 | 1 Jun 2018 | OPTICAL MATERIALS EXPRESS 1569
Optical Materials EXPRESS

Nearest-neighbor $sp^3d^5s^*$ tight-binding parameters based on the hybrid quasi-particle self-consistent GW method verified by modeling of type-II superlattices

Akitaka Sawamura,[1,*] Jun Otsuka,[1,2] Takashi Kato,[3] Takao Kotani,[2] and Satofumi Souma[4]

[1]*Analysis Technology Research Center, Sumitomo Electric Industries, Ltd., Yokohama 244-8588, Japan*
[2]*Department of Mechanical and Physical Engineering, Tottori University, Tottori 680-8552, Japan*
[3]*Transmission Device Laboratory, Sumitomo Electric Industries, Ltd., Yokohama 244-8588, Japan*
[4]*Department of Electrical and Electronic Engineering, Kobe University, Kobe 657-8501, Japan*
[*]*sawamura-akitaka@sei.co.jp*

Abstract: We report the determination of parameters in the nearest-neighbor $sp^3d^5s^*$ tight-binding (TB) model for nine binary compound semiconductors which consist of Al, Ga, or In and of P, As, or Sb based on the hybrid quasi-particle self-consistent GW (QSGW) calculations. We have used the determination parameters to calculate band structures and related properties of the compounds in the bulk phase relevant to mid-infrared applications and of the type-II (InAs)/(GaSb) superlattices. For the type-II (InAs)/(GaSb) superlattices with various superlattice periods, good agreement with photoluminescence measurements on the band gaps has been confirmed. Furthermore, two aspects of the band gap properties from other calculations have been reproduced: the band gap energies rising up to some superlattice periods and shrinking beyond them asymptotically. In both the bulk phase and the superlattices, erroneous flat valence bands have appeared within the nearest-neighbor sp^3s^* TB model. The present TB model has eliminated these artifacts, which are potential obstacles to design advanced superlattices.

OCIS codes: (040.3060) Infrared; (040.4200) Multiple quantum well; (040.6070) Solid state detectors; (160.1890) Detector materials; (160.6000) Semiconductor materials; (230.0250) Optoelectronics; (250.0040) Detectors.

References and links

1. H. Mohseni, M. Razeghi, G.J. Brown, and Y.S. Park, "High-performance InAs/GaSb superlattice photodiodes for the very long wavelength infrared range," Appl. Phys. Lett. **78**(15), 2107–2109 (2001).
2. H.J. Haugan, F. Szmulowicz, G.J. Brown, and K. Mahalingam, "Optimization of mid-infrared InAs/GaSb type-II superlattices," Appl. Phys. Lett. **84**(26), 5410–5412 (2004).
3. P. Delaunay, B.-M. Nguyen, D. Hoffmann, and M. Razeghi, "High-Performance Focal Plane Array Based on InAs-GaSb Superlattices With a 10-μm Cutoff Wavelength," IEEE J. Quantum Electron. **44**(5), 462–467 (2008).
4. H.J. Haugan, G.J. Brown, F. Szmulowicz, L. Grazulis, W.C. Mitchel, S. Elhamri, and W.D. Mitchell, "InAs/GaSb type-II superlattices for high performance mid-infrared detectors," J. Cryst. Growth **278**(1–4), 198–202 (2005).
5. G. J. Sullivan, A. Ikhlassi, J. Bergman, R.E. DeWames, J.R. Waldrop, C. Grein, M. Flatte, K. Mahalingam, H. Yang, M. Zhong, and M. Weimer, "Molecular beam epitaxy growth of high quantum efficiency InAs/GaSb superlattice detectors," J. Vac. Sci. Technol. B **23**(3), 1144–1148 (2005).
6. Council of the European Union, "Directive 2002/95/EC of the European Parliament and of the Council of 27 January 2003 on the restriction of the use of certain hazardous substances in electrical and electronic equipment," Off. J. Eur. Union L37, 19–23 (2003). https://eur-lex.europa.eu/legal-content/EN/TXT/?uri=CELEX:32002L0095
7. M. Razeghi, A. Haddadi, A. M. Hoang, C. Chen, S. Bogdanov, S. R. Darvish, F. Callawaert, R. McClintock, "Advances in antimonide-based Type-II superlattices for infrared detection and imaging at center for quantum devices," Infrared Phys. Tech. **59**, 41–52 (2013).
8. H. Mohseni, V. I. Litvinov, and M. Razeghi, "Interface-induced suppression of the Auger recombination in type-II InAs/GaSb superlattices," Phys. Rev. B **58**(23), 15378–15380 (1998)
9. J. L. Johnson, L. A. Samoska, A. C. Gossard, J. L. Merz, M. D. Jack, G. R. Chapman, B. A. Baumgratz, K. Kosai, and S. M. Johnson, "Electrical and optical properties of infrared photodiodes using the InAs/$Ga_{1-x}In_xSb$ superlattice in

#320348 https://doi.org/10.1364/OME.8.001569
Journal © 2018 Received 31 Jan 2018; revised 23 Mar 2018; accepted 11 Apr 2018; published 18 May 2018

Optical Materials EXPRESS

heterojunctions with GaSb," J. Appl. Phys. **80**(2), 1116–1127 (1996).
10. F. Fuchs, U. Weimer, W. Pletschen, J. Schmitz, E. Ahlswede, M. Walther, J. Wagner, and P. Koidl, "High performance InAs/$Ga_{1-x}In_xSb$ superlattice infrared photodiodes," Appl. Phys. Lett. **71**(22), 3251–3253 (1997).
11. C. H. Grein, H. Cruz, M. E. Flatté, and H. Ehrenreich, "Theoretical performance of very long wavelength InAs/$In_xGa_{1-x}Sb$ superlattice based infrared detectors," Appl. Phys. Lett. **65**(20), 2530–2532 (1994).
12. D.-J. Jang, M. E. Flatté, C. H. Grein, J. T. Olesberg, T. C. Hasenberg, and T. F. Boggess, "Temperature dependence of Auger recombination in a multilayer narrow-band-gap superlattice," Phys. Rev. B **58**(19), 13047–13054 (1998).
13. C. H. Grein, M. E. Flatté, J. T. Olesberg, S. A. Anson, L. Zhang, and T. F. Boggess, "Auger recombination in narrow-gap semiconductor superlattices incorporating antimony," J. Appl. Phys. **92**(12), 7311–7316 (2002).
14. P. Hoenberg and W. Kohn, "Inhomogeneous Electron Gas," Phys. Rev. **136**(3B), B864–B870 (1964).
15. W. Kohn and L. J. Sham, "Self-Consistent Equations Including Exchange and Correlation Effects," Phys. Rev. **140**(4A), A1133–A1138 (1965).
16. L. Hedin, "New Method for Calculating the One-Particle Green's Function with Application to the Electron-Gas Problem," Phys. Rev. **139**(3A), A796–A822 (1965).
17. J. Otsuka, T. Kato, H. Sakakibara, and T. Kotani, "Band structures for short-period $(InAs)_n(GaSb)_n$ superlattices calculated by the quasiparticle self-consistent GW method," Jpn. J. Appl. Phys. **56**(2), 021201 (2017).
18. D. Deguchi, K. Sato, H. Kino, and T. Kotani, "Accurate energy bands calculated by the hybrid quasiparticle self-consistent GW method implemented in the ecalj package," Jpn. J. Appl. Phys. **55**(5), 051201 (2016).
19. S. V. Faleev, M. van Schilfgaarde, and T. Kotani, "All-Electron Self-Consistent GW Approximation: Application to Si, MnO, and NiO," Phys. Rev. Lett. **93**(12), 126406 (2004).
20. A. N. Chantis, M. van Schilfgaarde, and T. Kotani, "*Ab Initio* Prediction of Conduction Band Spin Splitting in Zinc Blende Semiconductors," Phys. Rev. Lett. **96**(8), 086405 (2006).
21. T. Kotani, M. van Schilfgaarde, and S. V. Faleev, "Quasiparticle self-consistent GW method: A basis for the independent-particle approximation," Phys. Rev. B. **76**(16), 165106 (2007).
22. T. Kotani and H. Kino, "Linearized Augmented Plane-Wave and Muffin-Tin Orbital Method with the PBE Exchange-Correlation: Applied to Molecules from H_2 through Kr_2," J. Phys. Soc. Jpn. **82**(12), 124714 (2013).
23. T. Kotani, "Quasiparticle Self-Consistent GW Method Based on the Augmented Plane-Wave and Muffin-Tin Orbital Method," J. Phys. Soc. Jpn. **83**(9), 094711 (2014).
24. T. Kotani, H. Kino, and H. Akai, "Formulation of the Augmented Plane-Wave and Muffin-Tin Orbital Method," J. Phys. Soc. Jpn. **84**(3), 034702 (2015).
25. A. Sawamura, J. Otsuka, T. Kato, and T. Kotani, "Nearest-neighbor sp^3s^* tight-binding parameters based on the hybrid quasi-particle self-consistent GW method verified by modeling of type-II superlattices," J. Appl. Phys. **121**(23), 235704 (2017).
26. J. C. Slater and G. F. Koster, "Simplified LCAO Method for the Periodic Potential Problem," Phys. Rev. **94**(6), 1498–1542 (1954).
27. W. A. Harrison, *Electronic Structure and the Properties of Solids* (Dover, 1989).
28. J. Chadi, "Spin-orbit splitting in crystalline and compositionally disordered semiconductors," Phys. Rev. B **16**(2), 790–796 (1977).
29. P. Vogl, H. P. Hjalmarson, and J. D. Dow, "A semi-empirical tight-binding theory of the electronic structure of semiconductors," J. Phys. Chem. Sol. **44**(6), 365–378 (1983).
30. G. Klimeck, R. C. Bowen, T. B. Boykin, and T. A. Cwik, "sp^3s^* Tight-binding parameters for transport simulations in compound semiconductors," Superlatt. Microst. **27**(5/6), 519–524 (2000).
31. P. Charbonneau, "Genetic algorithms in astronomy and astrophysics," Astrophys. J. Suppl. Ser. **101**(2), 309–334 (1995).
32. P. Charbonneau and B. Knapp, "A user's guide to PIKAIA 1.0" (NCAR Technical Note 418+IA, 1995).
33. P. Charbonneau, "An introduction to genetic algorithms for numerical optimization" (NCAR Technical Note 450+IA, 2002).
34. P. Charbonneau, "Release notes for PIKAIA 1.2" (NCAR Technical Note 451+STR, 2002). http://www.hao.ucar.edu/modeling/pikaia/pikaia.php
35. T. B. Boykin, G. Klimeck, R. C. Bowen, and R. Lake, "Effective-mass reproducibility of the nearest-neighbor sp^3s^* models: Analytic results," Phys. Rev. B **56**(7), 4102–4107 (1997); Erratum in Phys. Rev. B **61**(7), 5033–5033 (2000).
36. G. Klimeck, R. C. Bowen, T. B. Boykin, and C. Salazar-Lazaro, T. A. Cwik, and A. Stoica, "Si tight-binding parameters from genetic algorithm fitting," Superlatt. Microst. **27**(2/3), 77–88 (2000).
37. T. B. Boykin, "Improved fits of the effective masses at Γ in the spin-orbit, second-nearest-neighbor sp^3s^* model: Results from analytic expressions," Phys. Rev. B **56**(15), 9613–9618 (1997).
38. J.-M. Jancu, R. Scholz, F. Beltram, and F. Bassani, "Empirical $spds^*$ tight-binding calculation for cubic semiconductors: General method and material parameters," Phys. Rev. B **57**(11), 6493–6507 (1998).
39. T.-T. Lu and L. J. Sham, "Valley-mixing effects in short-period superlattices," Phys. Rev. B **40**(8), 5567–5578 (1989).
40. R. Scholz, J.-M. Jancu, F. Beltram, and F. Bassani, "Calculation of electronic states in semiconductor heterostructures with an empirical $spds^*$ tight-binding model," Phys. Stat. Sol. (b) **217**(1), 449–460 (2000).
41. T. B. Boykin, G. Klimeck, and F. Oyafuso, "Valence band effective-mass expressions in the $sp^3d^5s^*$ empirical tight-binding model applied to a Si and Ge parametrization," Phys. Rev. B **69**(11), 115201 (2004).
42. B.-M. Nguyen, D. Goffman, R.-Y. Delaunay, E. K.-W. Huang, M. Razeghi, and J. Pellegrino, "Band edge tunability of

Optical Materials EXPRESS

M-structure for heterojunction design in Sb based type II superlattice photodiodes," Appl. Phys. Lett. **93**(16), 163502 (2008).
43. I. Vurgaftman, J. R. Meyer, and L. R. Ram-Mohan, "Band parameters for III-V compound semiconductors and their alloys," J. Appl. Phys. **89**(11), 5815–5875 (2001).
44. Y. Wei and M. Razeghi, "Modeling of type-II InAs/GaSb superlattices using an empirical tight-binding method and interface enginieering," Phys. Rev. B **69**(08), 085316 (2004).
45. S. Adachi, *Handbook on Physical Properties of Semiconductors, vol.2 III-V Compound Semiconductors* (Kluwer, 2004).
46. G. Kresse and J. Hafer, "Ab initio molecular dynamics for open-shell transition metals," Phys. Rev. B **48**(17), 13115–13118 (1993).
47. G. Kresse and J. Furthmüller, "Efficient iterative schemes for ab initio total-energy calculations using a plane-wave basis set," Phys. Rev. B **54**(16), 11169–11186 (1996).
48. G. Kresse and D. Joubert, "From ultrasoft pseudopotentials to the projector augmented-wave method," Phys. Rev. B **59**(3), 1758–1775 (1999).
49. S. Y. Ren, J. D. Dow, and D. J. Wolford, "Pressure dependence of deep levels in GaAs," Phys. Rev. B **25**(12), 7661–7765 (1982).
50. A. P. Ongstad, R. Kaspi, C. E. Moeller, M. L. Tilton, D. M. Gianardi, J. R. Chavez, and G. C. Dente, "Spectral blueshift and improved luminescent properties with increasing GaSb layer thickness in InAs-GaSb type-II superlattices," J. Appl. Phys. **89**(4), 2185–2188 (2001).
51. K. Miura, Transmission Device Laboratory, Sumitomo Electric Industries, Ltd., Yokohama 244-8588, Japan (unpublished, 2016).
52. P. Piquini, A. Zunger, and R. Margi, "Pseudopotential calculations of band gaps and band edges of short-period $(InAs)_n/(GaSb)_m$ superlattices with different substrates, layer orientations, and interfacial bonds," Phys. Rev. B **77**(11), 115314 (2008).
53. T. Kato and S. Souma, "sp^3s^* tight-binding calculations of band edges and effective masses of InAs/GaSb superlattices with different interface structures" (to be submitted).

1. Introduction

The development of mid-infrared sensors in wavelength range from 3 to 20μm is actively underway [1–5], because the normal vibrational energies of many molecules overlap mid-infrared. Sensors made of HgCdTe have been conventionally used. However, this approach has disadvantages, containment of hazardous heavy metals, Hg and Cd [6], the requirement of large-scale equipment for cryogenic cooling.

Type-II (InAs)/(GaSb) superlattices are expected to be alternative materials [7]. The type-II (InAs)/(GaSb) superlattice is characterized by larger electron and hole effective masses, which leads to reduction of dark current, lower sensitivity to compositional non-uniformity, and a wide ranging band gap accurately determined by controlling supertlattice period [8–10]. Moreover, toward high temperature operation of infrared sensors, band structure engineering is utilized to suppress Auger recombination [11–13].

There are several methods to predict band structure. Though density functional theory [14, 15] (DFT) is accepted as a reliable method, it is also known to underestimate a band gap notoriously, which is especially serious for semiconductors intended for infrared sensors. Theory beyond DFT, such as a GW method [16], can conquer this problem. We have calculated the band structures of type-II (InAs)/(GaSb) superlattices [17] using the latest version [18] of the hybrid quasiparticle self-consistent GW method (QSGW) [19–24] as implemented in ecalj package. A superlattice period is, however, still restricted to a far shorter value than that of real world sensors on account of heavy computational load.

This problem has led us to the previous study [25], where we have determined parameters of empirical tight-binding approach [26, 27] including spin-orbit interaction [28] within a nearest-neighbor sp^3s^* model [29, 30] based on the hybrid QSGW method by the help of genetic algorithm (GA) [31–34]. At that time, however, the nearest-neighbor sp^3s^* model is known to be accompanied by such a limitation as a poorly described transverse mass at the X point [35, 36], which is especially serious to aluminum compounds with conduction band minima at the X valley. The nearest-neighbor sp^3s^* model is therefore improved either by considering more distant interaction [37] or by adding d orbitals [38]; namely, the second-nearest-neighbor sp^3s^* and

Optical Materials EXPRESS

nearest-neighbor $sp^3d^5s^*$ models. Between these two improved models, while computationally more demanding on account of a doubled number of orbitals par atom, the latter is preferable from the viewpoint that the erroneous projection on the atomic symmetries is corrected [39], that the difference between masses of the electron and light hole is correctly reproduced [40], and that distortions, which may be encountered in superlattices, are handled more easily [41]. As mentioned later in Subsection 3.2, however, the known parameters for the nearest-neighbor $sp^3d^5s^*$ model by Jancu *et al.* [38] are short of accuracy when applied to the type-II (InAs)/(GaSb) superlattices.

In the present study we have extended our previous study by adopting the nearest-neighbor $sp^3d^5s^*$ model. The compound semiconductors taken into account are GaAs, InAs, GaSb, and InSb, whose parameters are necessary to treat the type-II (InAs)/(GaSb) superlattices, AlSb, which can serve as barrier layers in the mid-infrared sensors [7, 42, 43], and AlP, AlAs, GaP, and InP for completeness. Parameters of the aluminum compounds within the nearest-neighbor sp^3s^* model are also determined for comparison. Test calculations of the compounds in bulk phase and of the type-II (InAs)/(GaSb) superlattices have been also performed. We demonstrate that erroneous flat valence bands in the nearest-neighbor sp^3s^* model are eliminated. From here, we mean ours, not those in general or some other studies, by TB models, methods, parameters, or the like unless otherwise specified.

2. Method

Since an outline of a procedure to extract the TB parameters is almost the same as in our previous study, we describe it only briefly. The QSGW method in its infancy is known to overestimate the band gap [20, 21]. To remedy this problem, the exchange-correlation potential term is diluted [20] slightly with that of local density approximation [15]:

$$V^{\mathrm{XC}} = \alpha V^{\mathrm{XC}}_{\mathrm{QSGW}} + (1-\alpha)V^{\mathrm{XC}}_{\mathrm{LDA}}, \tag{1}$$

where α is an adjustable parameter. This hybrid QSGW method at $\alpha = 0.8$ is shown to describe energy band properties universally well for a wide variety of semiconductors and insulators [18]. In the present study, we have shifted α against each compound to reproduce accurately a band gap at the Γ point except that for AlP a band gap at the X point is considered, because with the Γ point α is not well adjusted. Specifically, after a lattice constant and band gap of a compound of interest are taken from Vurgaftman *et al.* [43] as input parameters for the hybrid QSGW method, α is so fixed that the specified and resultant band gaps agree at the specified lattice constant. Table 1 shows the specified lattice constants and fixed α's. At those input values, the energy band structures are calculated by the hybrid QSGW method along a pathway in the Brillouin zone adopted by Jancu *et al.* [38] and effective masses of the split-off hole, light hole, heavy hole, and electron at the Γ point are derived. For the light and heavy holes three orientations [100], [110], and [111] are considered. The target values subsequently fitted by the nearest-neighbor $sp^3d^5s^*$ model with all the TB parameters set to be adjusted by the GA include the energy levels along the pathway within an open interval

$$(\mathrm{VBM} - 2\mathrm{eV}, \mathrm{CBM} + 5\mathrm{eV}), \tag{2}$$

(1eV= 1.60218×10^{-19}J) where the VBM and CBM denote the valence band maximum and conduction band minimum, respectively, and the effective masses. Note that whereas in the nearest-neighbor sp^3s^* model setting some of the TB parameters to be adjusted by the GA suffices to determine them completely by virtue of exact analytic expressions which associate the energy band properties with the TB parameters [35], to our knowledge that is not the case in the nearest-neighbor $sp^3d^5s^*$ model because of lack of such expressions for compound semiconductors.

Optical Materials EXPRESS

Table 1. Input parameters employed in the hybrid QSGW calculations. The lattice constant a in Å(1Å= 1×10^{-10}m); the adjustable factor α in arbitrary unit. The parameters for gallium and indium compounds in our previous study are given again for reader's convenience.

	AlP	AlAs	AlSb	GaP	GaAs	GaSb	InP	InAs	InSb
a	5.4584	5.6524	6.1277	5.4417	5.6416	6.0817	5.8613	6.0501	6.4689
α	0.8644	0.7991	0.8367	0.8633	0.8319	0.7875	0.8393	0.8146	0.7631

3. Results

3.1. Parameters and bulk properties

The determined TB parameters are listed in Tables 2 and 3 for the aluminum and remaining compounds, respectively.

The corresponding main energies and effective masses of the compunds relevant to the mid-infrared sensors are summarized in Tables 4 to 8. The values from the hybrid QSGW and sp^3s^* TB calculations besides AlSb in our previous study are given again for reader's convenience. The properties are described slightly better by the $sp^3d^5s^*$ model except for the Γ_{7v} levels, probably because the exact analytic expressions which associate the properties with the TB parameters are unavailable as already mentioned. Since just comparing those limited properties may be insufficient to illustrate the quality of the $sp^3d^5s^*$ model, we show the band structures in Figs. 1 to 5. In AlSb as an example in Fig. 1, whereas the lowest conduction band is fitted moderately well by the sp^3s^* TB method along the left two segments ($L \rightarrow \Gamma \rightarrow X$) in the pathway, that is not the case further to the right than the first X point. In particular, the lowest valence band is almost flat between the X, W, and U, K points within the sp^3s^* TB method, reflecting the poorly described transverse mass. This deficiency is particularly serious to AlSb, because as evident in Fig. 1 an excited electron which should stay at the X valley may be incorrectly predicted to float along the wrong flat band. The $sp^3d^5s^*$ TB method resolves this problem because it fits the lowest conduction band well along the whole pathway, including the case of GaAs, GaSb, InAs, and InSb.

Optical Materials EXPRESS

Table 2. Tight-binding parameters for aluminum compounds in units of eV (1eV= 1.60218×10^{-19}J).

	AlP	AlAs	AlSb	AlP	AlAs	AlSb
		$sp^3d^5s^*$			sp^3s^*	
E_s^a	-5.7369	-5.3587	-5.4317	-11.1858	-19.2654	-17.4678
E_s^c	2.4768	1.1629	0.1469	2.6845	0.7389	-1.3600
E_p^a	3.4749	3.2294	3.5031	-0.0169	0.4576	0.5685
E_p^c	7.5792	6.1774	5.5066	7.0568	5.7634	3.8202
E_d^a	15.6194	14.3793	11.4645	–	–	–
E_d^c	15.0998	13.6899	12.2570	–	–	–
$E_{s^*}^a$	21.4604	21.5491	14.9250	91.9611	19.4509	132.5917
$E_{s^*}^c$	21.9365	19.296	17.1843	4.9536	5.9795	5.1388
$ss\sigma$	-1.2865	-1.5117	-1.6046	-1.3219	-1.8163	-2.1560
$s^*s^*\sigma$	-4.2741	-3.7528	-2.1411	–	–	–
$s_a^*s_c\sigma$	-0.7065	-1.2928	-0.3547	–	–	–
$s_as_c^*\sigma$	-1.8970	-3.0388	-2.9859	–	–	–
$s_ap_c\sigma$	1.8356	2.8162	1.8899	1.7233	2.8217	2.6362
$s_cp_a\sigma$	3.6594	2.4873	2.4073	2.5509	2.7552	2.5904
$s_a^*p_c\sigma$	2.1363	0.5349	1.5483	9.7581	4.2881	10.2872
$s_c^*p_a\sigma$	3.0947	0.2779	0.8846	2.7838	2.7552	2.5912
$s_ad_c\sigma$	-4.0983	-3.3367	-3.2156	–	–	–
$s_cd_a\sigma$	-2.8411	-3.1987	-3.6134	–	–	–
$s_a^*d_c\sigma$	-2.3281	-1.9115	-0.7865	–	–	–
$s_c^*d_a\sigma$	-2.1501	-1.2515	-2.2190	–	–	–
$pp\sigma$	4.4559	4.0510	3.8014	2.5463	2.8723	2.7676
$pp\pi$	-1.1822	-1.0976	-1.0774	-1.2132	-0.7586	-0.7182
$p_ad_c\sigma$	-0.8782	-1.5440	-1.9068	–	–	–
$p_cd_a\sigma$	-2.6314	-2.3183	-3.1393	–	–	–
$p_ad_c\pi$	1.5279	1.4130	0.9270	–	–	–
$p_cd_a\pi$	2.2382	1.5937	1.3943	–	–	–
$dd\sigma$	-1.4366	-1.4459	-0.4715	–	–	–
$dd\pi$	2.6870	3.0344	3.6027	–	–	–
$dd\delta$	-2.7939	-2.0065	-1.7187	–	–	–
$\Delta_a/3$	0.0129	0.1410	0.3598	0.0205	0.1087	0.2617
$\Delta_c/3$	0.0121	0.0175	0.0186	0.0093	0.0019	-0.0249

Optical Materials EXPRESS

Table 3. Same as Table 2 except that only the $sp^3d^5s^*$ model is dealt with for the gallium and indium compounds.

	GaP	GaAs	GaSb	InP	InAs	InSb
E_s^a	-6.2150	-6.1973	-4.9090	-4.9766	-5.6648	-5.7042
E_s^c	0.3609	-0.2237	-0.2994	0.1068	-0.2583	0.0071
E_p^a	3.2079	2.8611	3.4928	2.7952	3.6412	2.8443
E_p^c	6.5372	6.0223	5.8153	5.9043	5.4428	6.1200
E_d^a	14.9951	12.7596	11.4776	13.8323	12.8510	11.1852
E_d^c	14.6453	13.6722	12.8194	12.9168	13.4309	10.7393
$E_{s^*}^a$	19.2180	19.2807	16.6255	20.1936	18.2846	16.8739
$E_{s^*}^c$	20.8011	19.4917	17.9284	18.7500	17.5940	15.3779
$ss\sigma$	-1.6727	-1.1316	-1.0923	-1.0953	-1.0424	-0.5438
$s^*s^*\sigma$	-5.0184	-2.0202	-3.2277	-4.9283	-2.2986	-3.9129
$s_a^*s_c\sigma$	-1.3562	-0.9087	-0.4380	-0.9165	-1.1236	-0.1725
$s_as_c^*\sigma$	-3.0974	-1.4598	-3.3564	-2.9356	-3.1810	-2.6837
$s_ap_c\sigma$	3.0436	2.3411	2.8013	3.0329	2.9291	3.1504
$s_cp_a\sigma$	2.3692	2.2788	2.1263	1.9681	1.8408	2.1375
$s_a^*p_c\sigma$	0.5072	0.5816	2.2820	1.1163	2.9935	1.5058
$s_c^*p_a\sigma$	0.6914	0.2146	0.5854	0.9064	1.2504	2.1517
$s_ad_c\sigma$	-3.8048	-4.5328	-3.1243	-3.6861	-3.7194	-3.9271
$s_cd_a\sigma$	-2.9408	-2.6436	-2.5135	-3.0201	-3.2657	-2.0953
$s_a^*d_c\sigma$	-1.3178	-1.4745	-0.4088	-0.7530	-1.2525	-0.7380
$s_c^*d_a\sigma$	-1.2959	-1.1988	-1.1033	-2.4643	-1.1698	0.6081
$pp\sigma$	4.3849	4.1843	4.1210	3.9017	3.8430	3.7413
$pp\pi$	-1.3011	-1.1640	-1.5181	-0.9863	-0.9976	-1.3278
$p_ad_c\sigma$	-1.4936	-0.7827	-2.3517	-0.9146	-1.6600	-1.8410
$p_cd_a\sigma$	-2.4183	-2.6167	-2.2086	-2.7718	-3.6682	-2.5767
$p_ad_c\pi$	1.2677	1.1135	1.7161	0.8296	0.9864	0.9495
$p_cd_a\pi$	2.1779	1.8458	1.9519	1.3465	0.7884	1.9491
$dd\sigma$	-0.8525	0.0577	-1.9808	-1.3804	-0.5417	-2.3711
$dd\pi$	2.7334	2.6516	3.3149	2.9123	3.4663	2.8662
$dd\delta$	-2.4925	-2.3066	-1.1191	-2.2435	-2.3433	-1.0811
$\Delta_a/3$	0.0352	0.1497	0.4326	0.0434	0.1862	0.4207
$\Delta_c/3$	0.0703	0.0295	0.0173	0.1433	0.1580	0.0935

Optical Materials EXPRESS

Table 4. Bulk material properties of AlSb obtained by the hybrid QSGW and TB calculations. Energies are in units of eV; masses in terms of the free electron mass.

	QSGW	TB $sp^3d^5s^*$	TB sp^3s^*
Γ_{7v}	-0.651	-0.469	-0.652
Γ_{6c}	2.385	2.385	2.386
Γ_{7c}	3.599	3.191	4.567
Γ_{8c}	3.658	3.700	4.625
X_{6v}	-2.721	-2.729	-2.909
X_{7v}	-2.442	-2.341	-2.549
X_{6c}	1.470	1.470	1.472
X_{7c}	1.737	1.738	1.721
L_{6v}	-1.371	-1.363	-1.588
L_{7v}	-1.007	-1.009	-1.224
L_{6c}	1.842	1.842	1.920
m^*_{so}	-0.246	-0.203	-0.200
$m^*_{lh}[100]$	-0.132	-0.128	-0.106
$m^*_{lh}[110]$	-0.110	-0.109	-0.097
$m^*_{lh}[111]$	-0.105	-0.105	-0.095
$m^*_{hh}[100]$	-0.315	-0.323	-0.413
$m^*_{hh}[110]$	-0.600	-0.586	-0.653
$m^*_{hh}[111]$	-0.783	-0.743	-0.786
m^*_e	0.114	0.112	0.150

Table 5. Same as Table 4 except for GaAs.

	QSGW	TB $sp^3d^5s^*$	TB sp^3s^*
Γ_{7v}	-0.339	-0.250	-0.339
Γ_{6c}	1.519	1.520	1.519
Γ_{7c}	4.329	4.269	4.369
Γ_{8c}	4.510	4.510	4.550
X_{6v}	-3.044	-3.049	-3.236
X_{7v}	-2.964	-2.894	-3.111
X_{6c}	1.907	1.907	1.907
X_{7c}	2.232	2.228	2.285
L_{6v}	-1.445	-1.467	-1.638
L_{7v}	-1.240	-1.279	-1.432
L_{6c}	1.758	1.758	1.779
m^*_{so}	-0.169	-0.157	-0.150
$m^*_{lh}[100]$	-0.088	-0.088	-0.078
$m^*_{lh}[110]$	-0.078	-0.078	-0.072
$m^*_{lh}[111]$	-0.075	-0.076	-0.070
$m^*_{hh}[100]$	-0.315	-0.318	-0.362
$m^*_{hh}[110]$	-0.576	-0.587	-0.609
$m^*_{hh}[111]$	-0.767	-0.769	-0.763
m^*_e	0.069	0.069	0.079

Optical Materials EXPRESS

Table 6. Same as Table 4 except for GaSb.

	QSGW	TB $sp^3d^5s^*$	TB sp^3s^*
Γ_{7v}	-0.673	-0.770	-0.673
Γ_{6c}	0.812	0.800	0.812
Γ_{7c}	2.951	2.813	2.753
Γ_{8c}	3.158	3.145	2.960
X_{6v}	-3.130	-3.415	-3.422
X_{7v}	-2.887	-2.941	-2.164
X_{6c}	1.042	1.027	1.006
X_{7c}	1.293	1.284	1.289
L_{6v}	-1.671	-1.645	-1.749
L_{7v}	-1.272	-1.140	-1.371
L_{6c}	0.792	0.777	0.868
m^*_{so}	-0.145	-0.148	-0.121
$m^*_{lh}[100]$	-0.050	-0.052	-0.046
$m^*_{lh}[110]$	-0.046	-0.047	-0.049
$m^*_{lh}[111]$	-0.044	-0.045	-0.041
$m^*_{hh}[100]$	-0.229	-0.232	-0.246
$m^*_{hh}[110]$	-0.424	-0.436	-0.458
$m^*_{hh}[111]$	-0.565	-0.585	-0.616
m^*_e	0.045	0.044	0.049

Table 7. Same as Table 4 except for InAs.

	QSGW	TB $sp^3d^5s^*$	TB sp^3s^*
Γ_{7v}	-0.345	-0.433	-0.345
Γ_{6c}	0.417	0.418	0.417
Γ_{7c}	4.201	4.211	4.168
Γ_{8c}	4.640	4.639	4.323
X_{6v}	-2.618	-2.617	-2.970
X_{7v}	-2.612	-2.569	-2.900
X_{6c}	1.897	1.896	1.871
X_{7c}	2.534	2.534	3.316
L_{6v}	-1.305	-1.353	-1.416
L_{7v}	-1.058	-1.036	-1.535
L_{6c}	1.495	1.495	1.535
m^*_{so}	-0.105	-0.115	-0.097
$m^*_{lh}[100]$	-0.032	-0.032	-0.032
$m^*_{lh}[110]$	-0.031	-0.031	-0.031
$m^*_{lh}[111]$	-0.031	-0.031	-0.030
$m^*_{hh}[100]$	-0.344	-0.335	-0.349
$m^*_{hh}[110]$	-0.623	-0.583	-0.634
$m^*_{hh}[111]$	-0.850	-0.762	-0.854
m^*_e	0.027	0.027	0.027

Optical Materials EXPRESS

Table 8. Same as Table 4 except for InSb.

	QSGW	TB $sp^3d^5s^*$	TB sp^3s^*
Γ_{7v}	-0.731	-0.684	-0.731
Γ_{6c}	0.235	0.232	0.235
Γ_{7c}	2.921	2.717	2.812
Γ_{8c}	3.319	3.317	3.210
X_{6v}	-2.749	-2.997	-3.065
X_{7v}	-2.583	-2.580	-2.818
X_{6c}	1.381	1.379	1.369
X_{7c}	1.389	1.391	1.383
L_{6v}	-1.548	-1.506	-1.599
L_{7v}	-1.095	-0.989	-1.154
L_{6c}	0.763	0.762	0.786
m^*_{so}	-0.125	-0.108	-0.100
$m^*_{lh}[100]$	-0.018	-0.018	-0.017
$m^*_{lh}[110]$	-0.017	-0.018	-0.017
$m^*_{lh}[111]$	-0.017	-0.018	-0.016
$m^*_{hh}[100]$	-0.249	-0.256	-0.263
$m^*_{hh}[110]$	-0.468	-0.487	-0.498
$m^*_{hh}[111]$	-0.655	-0.684	-0.696
m^*_e	0.016	0.017	0.017

Optical Materials EXPRESS

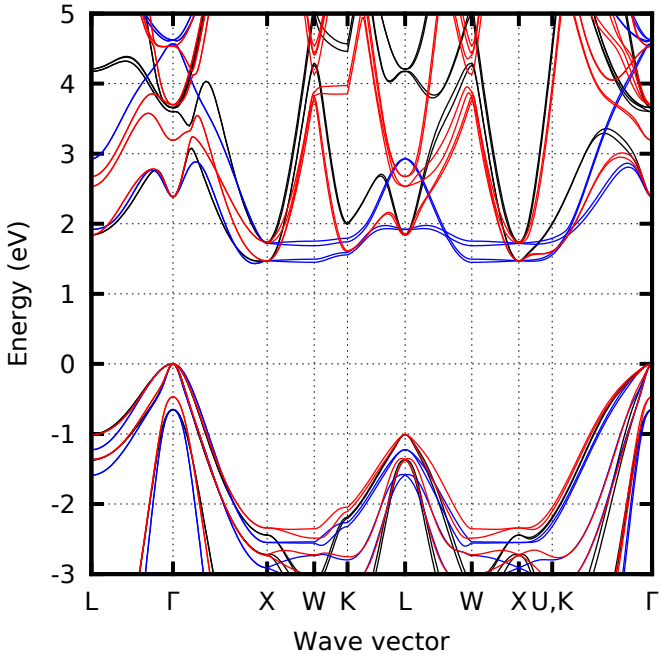

Fig. 1. Band structures of AlSb obtained by the hybrid QSGW (black) and TB calculations (blue for the sp^3s^* model and red for the $sp^3d^5s^*$ one). Energies are in units of eV.

3.2. Superlattice properties

Using the TB parameters for GaAs, InAs, GaSb, and InSb we have calculated the band gaps of a series of the (InAs)/(GaSb) and (InAs)/$(InSb)_1$/(GaSb) superlattices, assumed to be grown on GaSb substrates in a pseudomorphic way. The deformation of the InAs and interface layers is treated with classical elasticity [44]:

$$\begin{aligned} \epsilon^i_{xx} = \epsilon^i_{yy} &= \frac{a^{\text{sub}}}{a^i} - 1, \\ \epsilon^i_{zz} &= -\frac{2C^i_{12}}{C^i_{11}}\epsilon^i_{xx}, \end{aligned} \tag{3}$$

where ϵ^i_{xx}'s are the uniform strain in a material i made of two adjacent atomic layers, a^{sub} and a^i lattice constants of the substrate (GaSb) and material i, respectively, and C^i_{11} and C^i_{12} elastic constants of the material i. The lattice and elastic constants are taken from Refs. [43] and [45], respectively. No further atomic relaxation is considered. It should be noted that fractional coordinates of constituent atoms from such a classical elasticity and relaxed by generalized gradient approximation as implemented in Vienna Ab-initio Simulation Package [46–48] are in surprisingly good agreement [17]. The modifications of the TB parameters have been accounted for by including generalized Harrison's d^{-2} law [49]. Furthermore, the on-site energies of the d orbitals E_{xy}, E_{xz}, and E_{yz} are assumed to dependent linearly on the strain in the same way as proposed in Ref. [38]. The TB parameters related to the strain will be shown elsewhere.

Figure 6 shows a whole comparison of the calculated band gap with the photoluminescence (PL) data for the (InAs)/(GaSb) and (InAs)/$(InSb)_1$/(GaSb) superlattices with various periods. The PL data in Fig. 6 are extrapolated into T = 0K after Ref. [50] for the (InAs)/(GaSb) and Ref. [51] for the (InAs)/$(InSb)_1$/(GaSb). The TB band gaps agree well with those of the PL in

Optical Materials EXPRESS

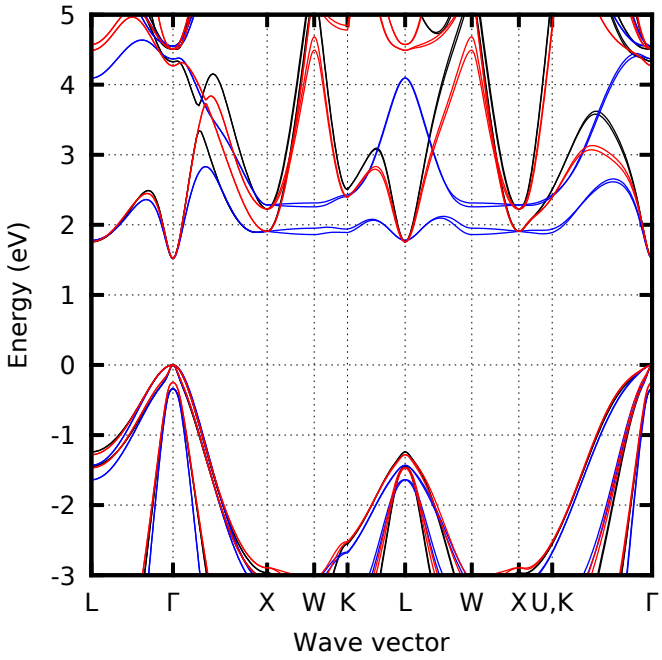

Fig. 2. Same as Fig. 1 except for GaAs.

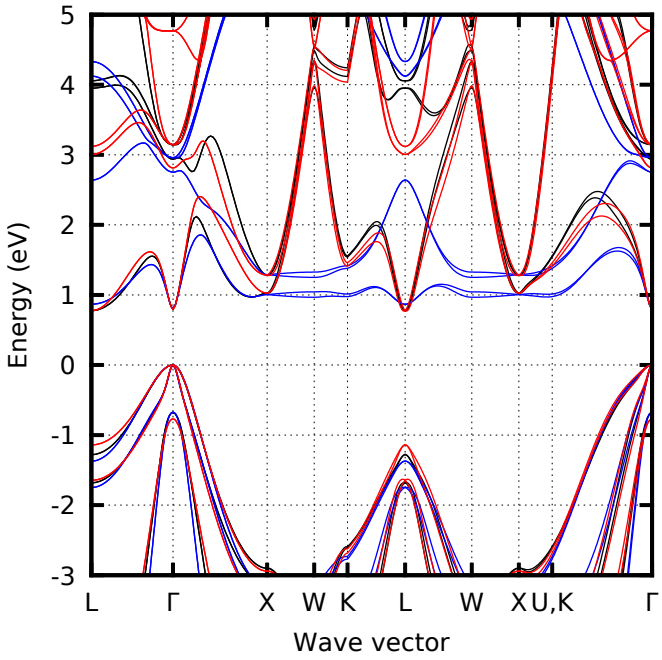

Fig. 3. Same as Fig. 1 except for GaSb.

Optical Materials EXPRESS

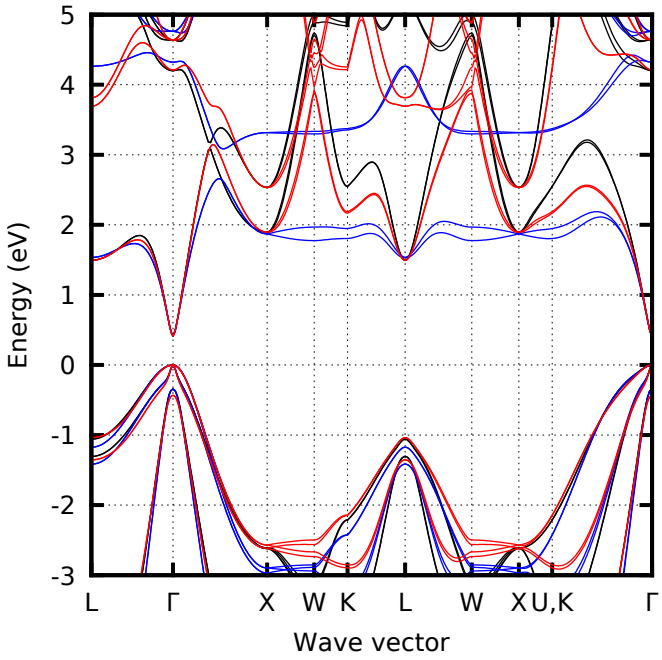

Fig. 4. Same as Fig. 1 except for InAs.

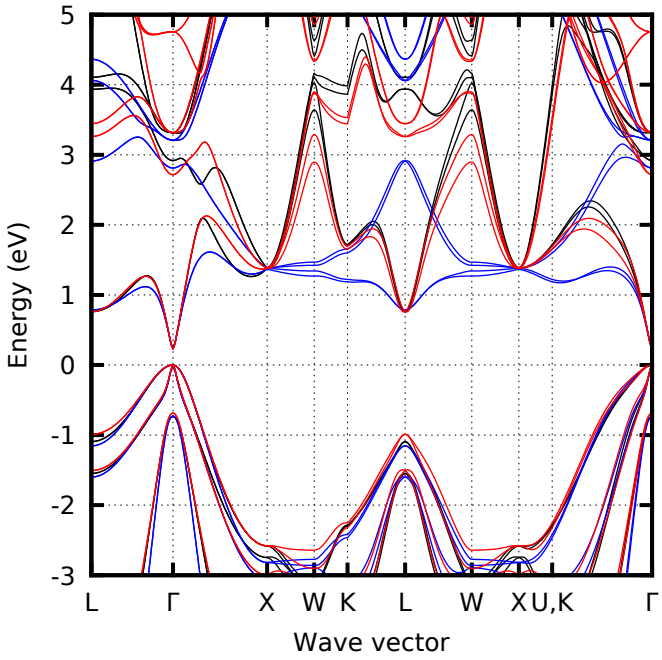

Fig. 5. Same as Fig. 1 except for InSb.

Optical Materials EXPRESS

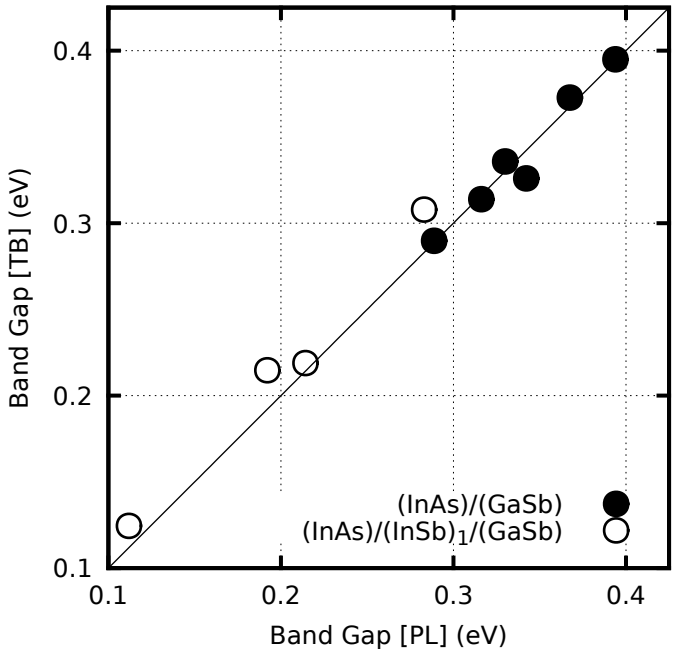

Fig. 6. Band gaps of (InAs)/(GaSb) (closed circle) and (InAs)/$(InSb)_1$/(GaSb) (open circle) with various superlattice periods calculated by the TB method compared with photoluminescence (PL) data extrapolated into $T = 0$K after Ref. [50] for (InAs)/(GaSb) and Ref. [51] for (InAs)/$(InSb)_1$/(GaSb). A diagonal line is drawn to guide the eye.

discrepancy of 16meV and 25meV for the (InAs)/(GaSb) and (InAs)/$(InSb)_1$/(GaSb) superlattices, respectively. The larger error for the latter may be attributed to large strain of 6% in bond length suffered by an InSb layer, which appears inevitably at the two interfaces.

More specifically, Figure 7 compares the band gap energies of the $(InAs)_n/(GaSb)_n$ superlattices in the TB model together with the results of the TB model parametrized by Jancu *et al.*, of empirical pseudopotential (EP) calculations [52], of the PL, and of the hybrid QSGW [17] method at $\alpha = 0.8$. First, all the empirical calculations show shrinking band gap energies in an asymptotic way with the superlattce period n sufficiently large, which is in line with the results of the PL and hybrid QSGW methods. Second, when we begin with $n = 1$, however, the band gap energies obtained by the hybrid QSGW and two TB methods exhibit bell lines, in other words, rise and then fall beyond some n's, with the EP method an exception. This findings will be discussed in detail elsewhere [53]. Third, as expected from Fig. 6, the present TB band gap energies reproduce the PL data well within one-third error compared to the other empirical methods. Difference between the hybrid QSGW and TB methods in the band gap energy itself may be attributed to impossibility to vary α in Eq.(1) spatially into a more appropriate value for each constituent material at least within the present implementation.

So far, we have mentioned an advantage of the $sp^3d^5s^*$ TB model over the other known one. Now we superpose the band structures of the $(InAs)_4/(GaSb)_4$ superlattice in Fig. 8 calculated by the sp^3s^* and $sp^3d^5s^*$ TB methods over that obtained by the hybrid QSGW method [17]. The modifications of the TB parameters have been accounted for by including Harrison's d^{-2} law in common for a fair comparison between the two TB models. The sp^3s^* TB model exhibits valence bands with almost flat dispersion between 1.0 and 1.5eV. Since these flat valence bands do not appear in the hybrid QSGW method, they are artifacts reflecting the similar flat valence bands in

Optical Materials EXPRESS

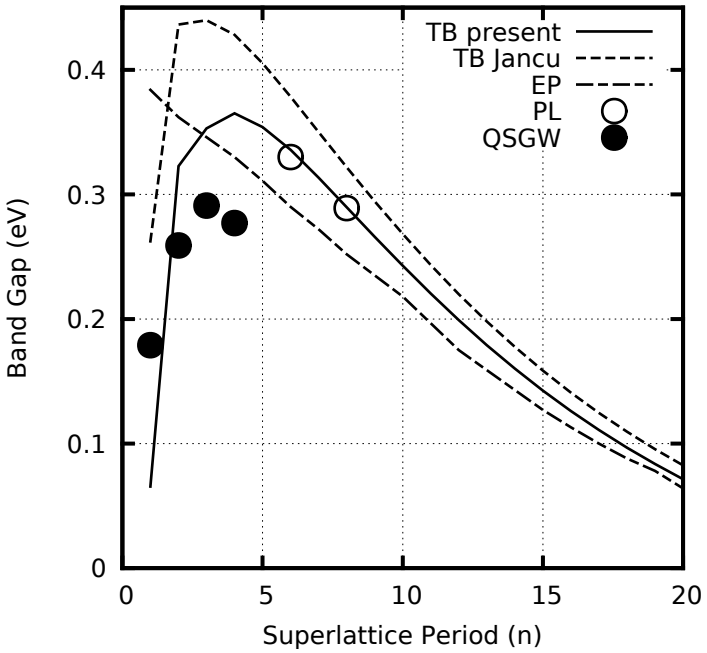

Fig. 7. Band gaps of superlattice $(InAs)_n/(GaSb)_n$ calculated by the TB method (solid line) compared with those calculated by the TB method in Ref. [38] (dashed line), with those calculated by the empirical pseudopotential (EP) method in Ref. [52] (dash-dotted line), and with photoluminescence (PL) data extrapolated into $T = 0$K after Ref. [51] (open circle), and with those calculated by the hybrid QSGW method [17] (closed circle).

the bulk band structures as explained in the previous subsection. On the other hand, the $sp^3d^5s^*$ model eliminates these artifacts. Although at the present stage these artifacts may seem harmless, that is not the case when designing the advanced superlattices including the barrier layers which consist of AlSb, whose erroneous energy levels around the X point in the bulk phase will be folded down into the Γ point and its neighborhood in the superlattices. Although one might hit upon applying the $sp^3d^5s^*$ model to the barrier layers and the sp^3s^* to the remaining layers, the interface between the different TB models would become hard to deal with. One should apply the $sp^3d^5s^*$ model to the superlattices including the barrier layers altogether.

4. Conclusion

We report determination of parameters in the $sp^3d^5s^*$ TB model for the nine binary compound semiconductors which consist of Al, Ga, or In and of P, As, or Sb based on the hybrid QSGW calculations. For the compounds in the bulk phase actually or potentially relevant to the type-II (InAs)/(GaSb) superlattices, we have confirmed that the erroneous flat valence bands, which appear within the sp^3s^* TB model, are eliminated. We have confirmed that the band gap energies of the type-II (InAs)/(GaSb) superlattices of various superlattice periods using the present $sp^3d^5s^*$ TB model agree with those of the corresponding PL data within discrepancy of 25meV. We have further compared the band gap energies of the type-II (InAs)/(GaSb) superlattices of common superlattice periods for each layer calculated by the present TB model with those calculated using the other known TB model, the EP method, and the hybrid QSGW method and with the PL data. The TB model reproduces an asymptotic decrease in the band gap energies for the large superlattice period obtained by the other TB and the EP methods and a bell line for the small

Optical Materials EXPRESS

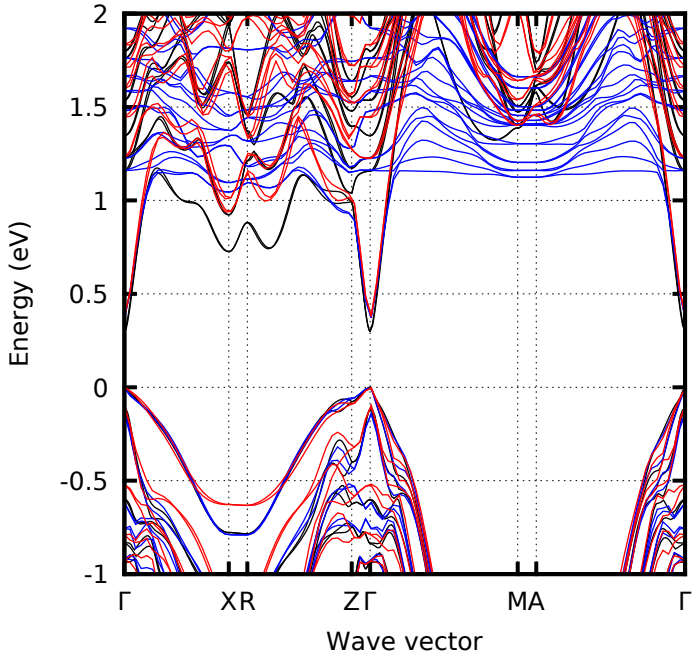

Fig. 8. The band structure of $(InAs)_4/(GaSb)_4$ superlattice obtained by the hybrid QSGW (black) and TB methods (blue for the sp^3s^* model and red for the $sp^3d^5s^*$ one). See Ref [17] for the complete results of the hybrid QSGW method.

superlattice period predicted by the other TB and the hybrid QSGW methods. The band gap energies calculated by the present TB model agree best with the PL data. Moreover, last but not least, the erroneous flat valence bands, which are potentially harmful to design the barrier layers, within the sp^3s^* TB model are eliminated using the present $sp^3d^5s^*$ TB model again along with the bulk phase. The present results indicate that the TB model is a reliable method to guide the superlattice design.

Acknowledgments

The authors are grateful to M. Shiozaki and Dr. A. Yamaguchi for helpful suggestions and encouragement and acknowledge the computing time provided by the Computing System for Research in Kyushu University.